# Laboratory testing and model calibration of a crushed stone backfill in a geosynthetic reinforced soil wall

*Chukwuma* Okafor[1], *Sam* Dunlop[1], *Brian* Anderson[1], and *Jack* Montgomery[1]

[1] *Auburn University, Department of Civil and Environmental Engineering, 205 W. Magnolia Ave, Auburn, , AL 36849, USA*

[#]*Corresponding author: cco0013@auburn.edu*

## ABSTRACT

The objective of this study was to understand the effect of the choice of backfill constitutive models on the numerical simulation of a geosynthetic reinforced soil-integrated bridge system (GRS-IBS). The #89 material, a crushed angular granite stone, characterized by maximum particle sizes of 9 mm, was used for the reinforced backfill for the retaining wall. Consolidated drained triaxial tests were conducted at confining stresses of 48 kPa, 83 kPa, and 117 kPa. The average friction angle was 42 degrees. Two soil models (the linear-elastic perfectly-plastic and the Hardening Soil) were calibrated using the laboratory test results. The calibrated soil models were then used to model the reinforced backfill material in finite element simulations of the abutment. Results of the calculated vertical stresses at the instrument position showed reasonable agreement with the field measurement. The non-linear model predicted about twice the deformation (lateral displacement and bridge seat settlement) compared to the linear-elastic perfectly plastic model. Settlement results showed maximum values corresponding to 0.22% and 0.45% of the abutment height for linear-elastic perfectly-plastic model and Hardening-Soil model, respectively, which are less than 0.5% limit recommended by US FHWA, while the lateral displacements were 0.22% and 0.44% of the abutment height for linear-elastic perfectly-plastic model and Hardening Soil model, respectively, both less than the 1% limit recommended by the US FHWA.

**Keywords:** numerical modelling; geosynthetics; retaining walls; laboratory testing.

## 1. Introduction

Appropriate material characterization is paramount in the solution of any geotechnical engineering problem as it informs the general behavior of a system (the total load input, load resistance/transfer, yielding, volume change, etc.). This is especially true for numerical models, which have become prevalent both in academic research and engineering practice. These models can offer an extensive insight into the response of geotechnical systems with the flexibility to study multiple scenarios and perform sensitivity studies, which would be more difficult to do using physical modelling or observations.

Constitutive models are critical to numerical analyses as they describe the material behavior in the form of mathematical expressions. When selecting a model, it is important to ensure the model can capture the key aspects of material behavior which control the scenario being modeled (Wood 2014). Calibration and validation at both the element scale and system level are needed to ensure that key aspects of a material behavior are accurately represented by a constitutive model. Calibration is commonly done using laboratory tests, in-situ tests, or a combination of both, while validation is done using carefully controlled physical models or well-characterized case histories.

The objective of this study was to calibrate the linear-elastic perfectly-plastic model and the Hardening Soil constitutive model implemented in Plaxis3D to lab data for a crushed stone backfill material. Compacted, crushed stone is commonly used in geotechnical practice, but there is relatively little discussion in literature on how to properly model this material. In this study, laboratory testing of the #89 backfill material, which is commonly used in Alabama, is discussed. The #89 material is a crushed angular granite stone, characterized by maximum particle sizes of about 9 mm. Two different constitutive models were used in this study for the backfill material: the linear-elastic (and perfectly plastic) model with Mohr-Coulomb failure criterion (referred to as Mohr-Coulomb or MC model hereafter, for brevity) and the elasto-plastic, non-linear Hardening Soil model (referred to as HS model hereafter). The steps taken to use the laboratory results to calibrate two constitutive models are also detailed.

The calibrated models were then used as a reinforced fill in a finite element model of a Geosynthetic Reinforced Soil-Integrated Bridge System (GRS-IBS), which was constructed in Marshall County, Alabama in 2018. Construction, instrumentation, and monitoring of the Marshall County GRS-IBS were documented in previous studies that assessed field performance of the structure (Hogan 2018, Hogan et al 2019, and Stallings 2020). In this study, these field measurements are compared with the simulations. The simulation results agree well with the stresses measured in the field and displacements predicted from the simulations are small as was observed during and after construction. For the current study, the MC provided reasonable results while being simpler to calibrate and run.

## 2. Laboratory Tests and Material Properties

The properties of the backfill material were determined using laboratory testing methods and the results were implemented in the numerical models.

Standard Proctor tests, conducted to simulate field compaction resulted in a compacted unit weight of 16.5 kN/m$^3$ for the backfill. Sieve analysis results (Figure 1) showed zero fines content, with an effective grain size of 2.5 mm and maximum aggregate size of 9.5 mm (ALDOT 2017). The material is an angular crushed granite stone with free draining properties meeting Alabama Department of Transportation (ALDOT) design requirements. The coefficient of uniformity ($C_U$) was 2.746 and the coefficient of curvature ($C_C$) was 1.193.

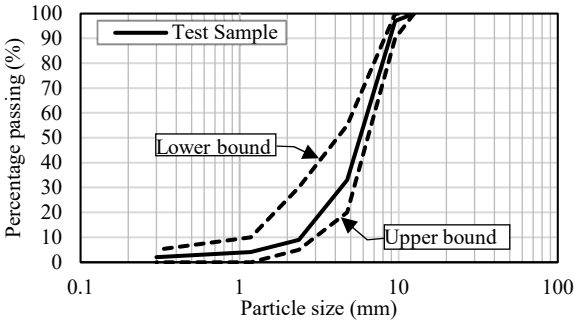


**Figure 1.** Plot of sieve analysis results.

Consolidated drained (CD) triaxial tests were used to estimate both the secant elastic modulus ($E_{50}$) of the soil and the friction angle. CD tests were performed at 48 kPa, 83 kPa, and 117 kPa to capture the expected range of in-situ stresses. Figure 2 shows a plot of the Mohr circles at failure for the tests at the various confining stresses. The average friction angle of the backfill material was 42 degrees while the cohesion intercept was zero (c'=0 kPa). Figure 3 shows the steps taken to calculate the secant modulus. The average secant modulus for the three different confining stresses was calculated as 18,200 kPa at strain of 1.00%.

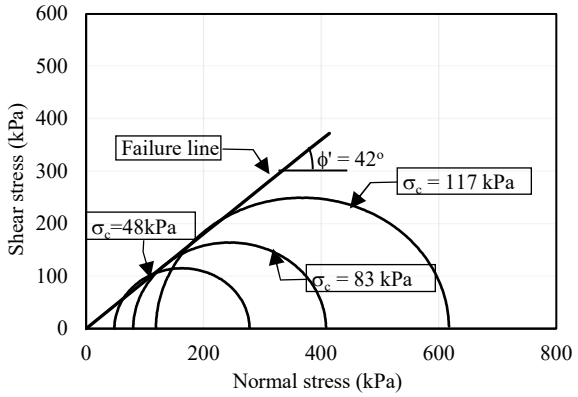


**Figure 2.** Mohr circles from consolidated drained triaxial tests.

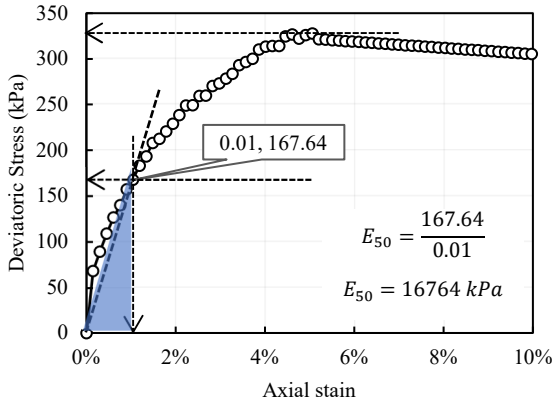


**Figure 3.** Illustrating the estimation of secant modulus.

## 3. Constitutive Model Calibration

Calibration of the constitutive models was performed using simulated triaxial test with the same test configurations as the laboratory tests using a single point algorithm via the built-in Plaxis SoilTest (Sloot 2018). The SoilTest program offers a concise approach to calibrate soil models to physically observed behaviors without the need to create a complete finite element model (Sloot 2018). The MC model used in this study is a linear elastic, perfectly plastic model and requires the user to select a Young's modulus ($E$), Poisson's ratio ($v$), cohesion ($c$), friction angle ($\phi$), and dilatancy angle ($\psi$).

The HS model is capable of simulating stress-dependency, unload-reload and non-linear stress-strain behavior of soils. The HS model simulates both shear hardening used to model irreversible strains due to primary deviatoric loading and compression hardening used to model irreversible plastic strains due to primary compression in oedometer and isotropic loading (Bentley 2021a). Additionally, the HS model simulates stress dependency according to a power law with the power as an input parameter $m$ (ranges from 0 to 1), elastic unloading and reloading, and failure according to the Mohr-Coulomb failure criterion (Bentley 2021a).

Other input parameters for calibrating the HS model include: the reference pressure ($p^{ref}$), the primary compression modulus ($E_{oed}^{ref}$), the reference stiffness corresponding to primary deviatoric loading ($E_{50}^{ref}$), the reference unloading/reloading Young's modulus corresponding to the reference pressure ($E_{ur}^{ref}$), the elastic Poisson ratio ($v_{ur}$), the ratio of the deviatoric stress at failure to the asymptote maximum deviatoric stress ($R_f$), as well as the Mohr-Coulomb failure criterion parameters. Table 1 shows the input data for the calibration of the HS model for 83 kPa confining stress.

The soil models were successfully calibrated to the laboratory data with reasonable agreement observed between the simulated and laboratory data points. Figure 4 depicts the measured and simulated stress-strain response for different confining stresses.

**Table 1.** Calibration input data for HS model at 83 kPa confining stress

| Parameter symbol | Units | Value | Note |
|---|---|---|---|
| $E_{50}^{ref}$ | kPa | 16800 | Calculated from CD triaxial test as shown in Figure 2. |
| $E_{oed}^{ref}$ | kPa | 13400 | $E_{oed}^{ref} \approx E_{50}^{ref}$ |
| $E_{ur}^{ref}$ | kPa | 50300 | Default value ( $E_{ur}^{ref} \approx 3E_{50}^{ref}$ ) |
| $m$ | - | 0.5 | Default value |
| $v_{ur}$ | - | 0.25 | |
| $K_o^{nc}$ | - | 0.33 | Default value ( $K_0^{nc} = 1 - \sin\phi$ ) |
| $p^{ref}$ | kPa | 82.7 | Taken as each confining stress level. |
| $c$ | kPa | 0 | Cohesionless soil |
| $\phi$ | ° | 42 | Estimated from triaxial testing |
| $\psi$ | ° | 12 | Default value ( $\psi^o = \phi^o - 30^o$ ) |
| $R_f$ | - | 0.84 | Iterated to fit laboratory data plots (default value = 0.9) |

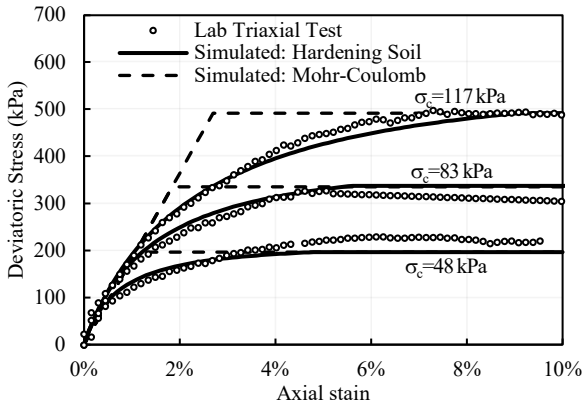


**Figure 4.** Simulated vs laboratory-measured stress-strain response for the # 89 gravel.

## 4. Numerical Modelling

The calibrated soil models for the #89 crushed stone backfill was used in numerical analyses of a geosynthetic reinforced soil-integrated bridge system (GRS-IBS), using Plaxis3D. A pseudo-2D model was created to simulate the Marshall County GRS-IBS and is presented in this study. The full 3D results are described by Okafor et al. (2023). The dimensions of the model and the locations of the various layers are shown in Figure 6, while the constitutive properties are listed in Table 2. The full construction process and description of each of the layers is provided by Hogan et al. (2019).

The soil volumes are modelled by means of 10-node tetrahedral elements with three degrees of freedom per node ($u_x$, $u_y$ and $u_z$). The generated mesh used for the analyses (Figure 5) had 8750 elements and 18596 nodes, with an average element size of 0.141 m. The geosynthetic layers were modelled using 6-node triangular surface element with three degrees of freedom per node (Bentley 2021b), with constant stiffness. Table 2 shows the input parameters for the GRS-IBS numerical model. The simulations modeled a realistic construction sequence, including excavation, sequential placement of lifts, and transient compaction loads. The final stages include distributed loads to represent the bridge beams (63 kPa) and traffic loading (12 kPa).

The interface between the backfill and the cut-slope, and the interface between the backfill and the facing units were modeled using zero-thickness, 12-node interface elements (Bentley 2021a). The properties for these elements are shown in Table 2, along with the references for the selected values. The interface between the facing units and the geosynthetic and the geosynthetic and the backfill were modeled using a strength reduction factor to capture the reduced strength properties.

A mesh sensitivity study was performed to examine the effects of mesh size on the numerical solution. Figure 6 compares the maximum bridge settlements from models with average element sizes that are 20% smaller and 50% and 80% bigger than the baseline mesh. The results are plotted versus the number of nodes in the model in Figure 6 and the maximum seat settlements from the solutions were normalized to the results from the model with the finest elements. The baseline mesh and the mesh with 20% smaller elements showed identical settlements, indicating that the model was sufficiently discretized. Coarser models showed higher settlements, but the difference for all models was within 10%. The calculation time for the different models was significantly different (Figure 6) with the finest mesh taking approximately 20% more time per run compared with the baseline model. All simulations were performed using a windows 10 64-bit computer with 20 processors @ 2.2 GHz each and 16 GB of RAM.

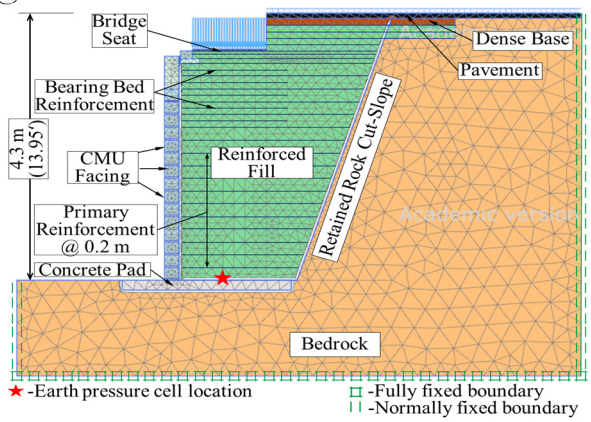


**Figure 5.** Generated mesh for the GRS-IBS model.

**Table 2.** Material properties used for the numerical simulations.

| Name | Input Properties |
|---|---|
| **Soil clusters:** | |
| # 89 Backfill | MC; $\gamma$=16.5 kN/m$^3$; =1.4 kPa; $\phi$ = 42$^o$; $\psi$=12$^o$; $E$=18200 kPa; $\nu$=0.25; $R_{inter}$ =0.8[d] |
| | HS; $\gamma$=16.49 kN/m$^3$; $c$=1.4 kPa; $\phi$=42$^o$; $\psi$=12$^o$; $E_{50}^{ref}$ =18200 kPa; $E_{oed}^{ref}$ =17200 kPa [a]; $E_{ur}^{ref}$ =55200 kPa [b]; $m$ = 0.5[c]; $R_{inter}$ =0.8[d] |
| Dense Base | LE; $\gamma$=24 kN/m$^3$; $E$=1.79x10$^6$ kPa; $\nu$=0.25; $R_{inter}$ =0.8 |
| Sandstone | LE; $\gamma$=24 kN/m$^3$; $E$=2.6x10$^6$ kPa; $\nu$=0.25. |
| CMU | LE; $\gamma$=12.5 kN/m$^3$; $E$=20 GPa; $\nu$=0; $R_{inter}$ =0.55[d] |
| CMU + #4 Rebar | LE; $\gamma$=16.3 kN/m$^3$ [e]; $E$=30 GPa [f]; $\nu$=0; $R_{inter}$ =1.0 |
| Concrete Pad | LE; $\gamma$=24 kN/m$^3$; $E$=23.6x10$^6$ kPa; $\nu$=0.3 |
| Pavement | LE; $\gamma$=22.8 kN/m$^3$; $E$=1.38x10$^6$ kPa; $\nu$=0.2; |
| **Geosynthetic:** | |
| Geogrid | Elastic (Constant Stiffness); Isotropic; $EA$= 434 kN/m [g] |
| **Interfaces:** | |
| Backfill-Retained | MC; $c$=0.7 kPa; $\delta_i$=30$^o$ [h]; $E$=4140 kPa; $\nu$=0.45. |
| CMU-Backfill | LE: $E$=18200 kPa; $\nu$=0.45. |

MC = Mohr-Coulomb, HS = Hardening Soil, LE = Linear Elastic, [a] Plaxis3D recommended, [b] $E_{ur}^{ref} \approx 3E_{50}^{ref}$ (Plaxis3D default), [c] Plaxis3D default, [d] after Abu-Farsakh et al. (2018), [e] & [f] ≈1.5 times CMU, [g] $J \approx \frac{T_{ult}}{\varepsilon_{ult}}$, [h] NAFVAC, 1982.

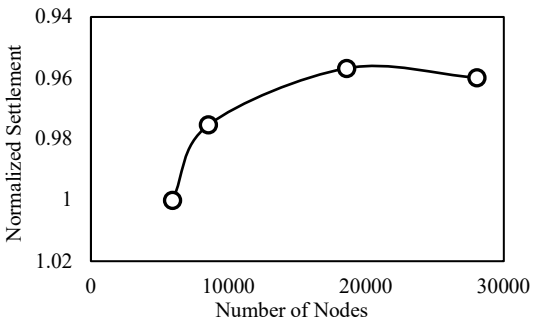


**Figure 6.** Mesh sensitivity analyses.

## 5. Results

The Marshall County GRS-IBS was instrumented with earth pressure cells and piezometers placed in the backfill and survey targets along the edges of the facing blocks for deformation monitoring. Details of the responses are presented by Stallings (2019). The numerical simulations were performed using both soil constitutive models described above. The simulation procedure was the same for both constitutive models. In this section, the simulation results are compared to each other to assess the effect of choice of constitutive model on the simulation results and to the field measurements to validate the simulation approach. Results are compared for stresses in the backfill, settlement of the bridge seat, lateral displacement of the facing and tensile forces and strains in the geosynthetic reinforcement.

### 5.1. Stresses in Backfill

Figure 8a shows the stress distribution at the base of the reinforced soil mass while Figure 8b shows the stress development at the instrument position versus wall height during construction. The earth pressure cell was placed 0.9 m from the facing units and was positioned at the center of the abutment length. The first readings were not collected using the backfill had reached a height of 3.8 m. The vertical stress in the backfill increased after this point and reached their maximum value (83 kPa) after the bridge was opened to traffic. The maximum vertical stress at the instrument position from the simulations was 83 kPa for the MC model and 77 kPa from the HS model. While the final stress magnitude was better predicted by the MC model, the stress build-up as the construction progressed had a better agreement with the predictions from the HS model (Figure 8b).

It is interesting to note that the maximum stress at the instrument location was less than would be calculated based on the height of the backfill and the surcharge load imposed by the bridge beams (Figure 7a). This reduced stress is likely caused by load shedding due to the geosynthetic-CMU interaction as reported by Hatami and Bathurst (2005). The simulations show that the stress at this height is near zero at the facing element and increased rapidly in the first 10 cm beyond the facing.

This load shedding can be better observed by examining the vertical stress contours within the backfill (Figure 8a for MC model, and 8b for the HS model). Figure 8 shows similar stress patterns for both soil models. The stress magnitude for zones close to the facings were zero, with stress intensity generally increasing towards the cut-slope. Zero-stress zones are located right behind the facing, but the impact of this shedding is limited to about 0.4 m from the back of the facing.

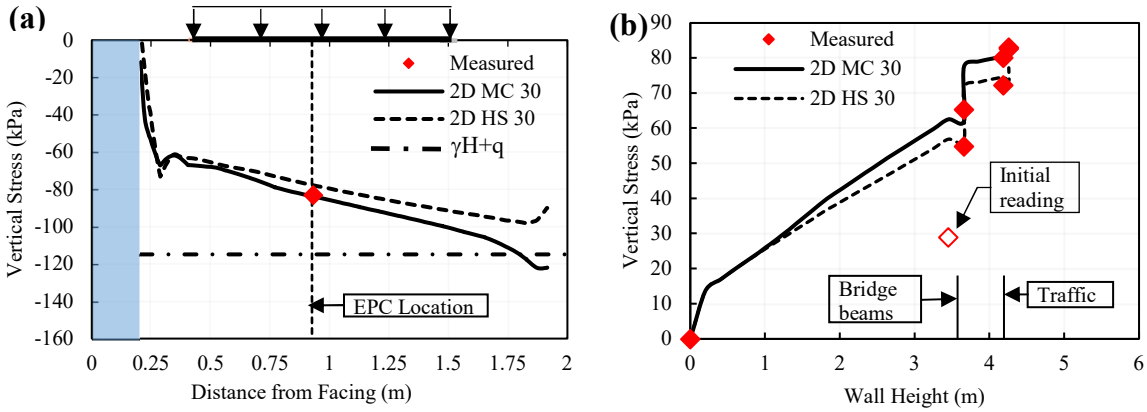


**Figure 7.** (a) Vertical stress distribution at wall foundation (b) vertical stress development at instrument position.

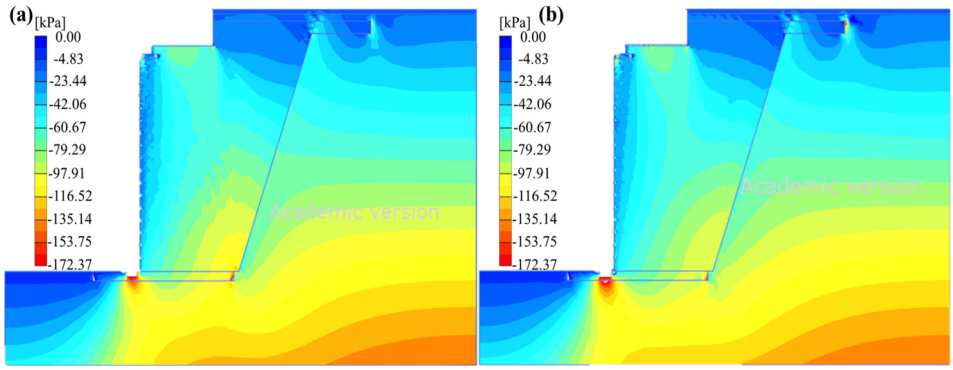


**Figure 8.** Vertical stress contours for (a) Mohr-Coulomb and (b) Hardening Soil models.

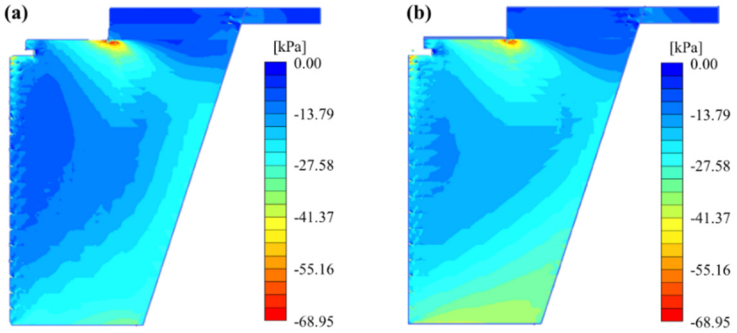


**Figure 9.** Horizontal stress contours for (a) Mohr-Coulomb and (b) Hardening Soil models with reinforced zone isolated

While the MC model showed a slightly higher stress magnitude (about 8% higher than the HS model) at the instrument location, the stress contours shown in Figure 8 depicts very similar stress patterns between the two constitutive models.

Figure 9 shows stress contours for the horizontal stresses in the backfill for both the MC model and the HS model. The horizontal stresses show similar stress pattern and magnitude, with the MC model showing slightly less intensity within the bearing bed reinforcement zone. This similarity in stress patterns and magnitudes is likely because the reinforced zone stayed primarily elastic throughout the construction and loading stages (Figure 10).

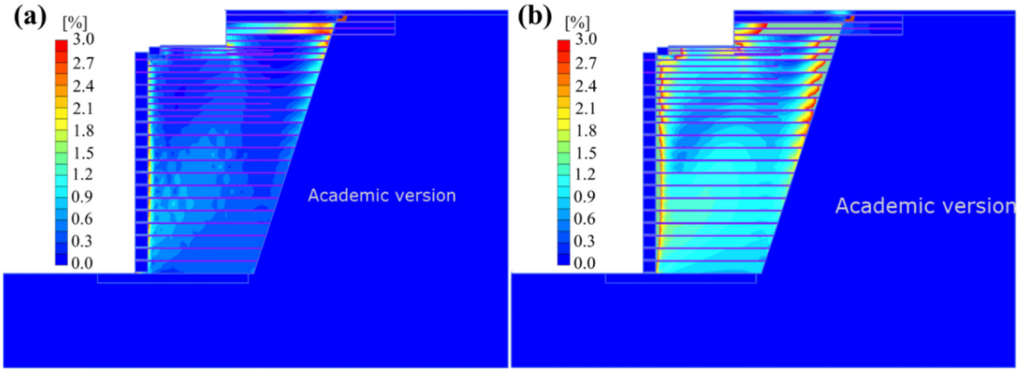


**Figure 10.** Shear strain contour plots for (a) Mohr-Coulomb and (b) Hardening Soil models.

Both models show maximum shear strains at interfaces between the backfill and the cut-slope and between the facing units and the backfill. Generally, the HS model showed strain magnitudes about two times more than that of the MC model. This is because the MC model has a stiffer stress-strain response for the ranges of stresses observed, and the HS model strains about twice as much to reach these stresses, i.e., for a similar stress magnitude (e.g. $\sigma_c$ of 83 kPa, Figure 4), the strain at failure for the MC model was 2% while the strain at failure for the HS model for the same stress was 4%.

## 5.2. Bridge seat settlement

The GRS-IBS was built on sandstone bedrock and as expected, there were no settlement at the foundation level. Recommendations from Adams et al. (2012) limit the settlement to 0.5% of the wall or abutment height. Monitoring of the wall settlement was performed during construction and for a period of 26 months after the bridge was opened. These surveys were performed using a total station and details on the methodology and the results are discussed by Stallings (2020). There was significant noise in the surveys, but the observed settlement was less than 20 mm.

Figure 11 shows the cumulative bridge seat settlement from the simulations. Recommendation for estimation of settlements in the design guideline by Adams et al. (2012) is based on vertical stresses due to the dead loads before the bridge is open, hence, results are presented herein for settlements due to dead loads, and then after application of traffic loads.

The maximum settlements from the dead loads were 7.80 mm and 16.26 mm, which were about 0.22% and 0.45% of the abutment height for the MC model and the HS model respectively, both less than the 0.5% limit recommended by the United States Federal Highway Administration (US FHWA) guidelines (Adams et al. 2012).

The maximum settlements from all construction stages until the structure was opened to traffic were 9.41 mm and 19.38 mm, which were about 0.23% and 0.36% of the GRS-IBS height for the MC model and the HS model respectively, again, less than the 0.5% limit recommended by the US FHWA guidelines (Adams et al. 2012).

Figure 12 shows the vertical displacement contours for the two soil models. Both models show very similar displacement patterns with most of the settlement occurring within the bearing bed reinforcement, this is likely because of the extra secondary reinforcement placed within the bearing bed. However, the HS model produced displacement magnitudes about twice that of the MC model, this, as observed for the strain results, is because the MC model has a stiffer stress-strain response, and the HS model strains about twice as much for the observed stress ranges.

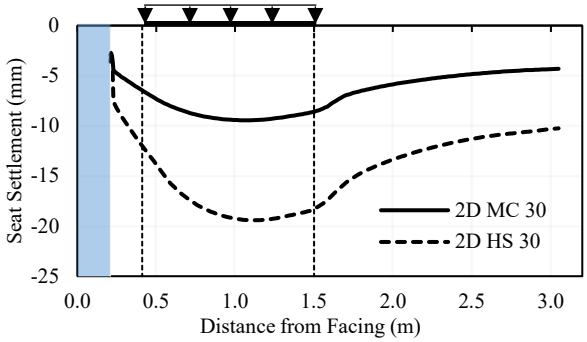


**Figure 11.** Settlement vs distance from back of facing.

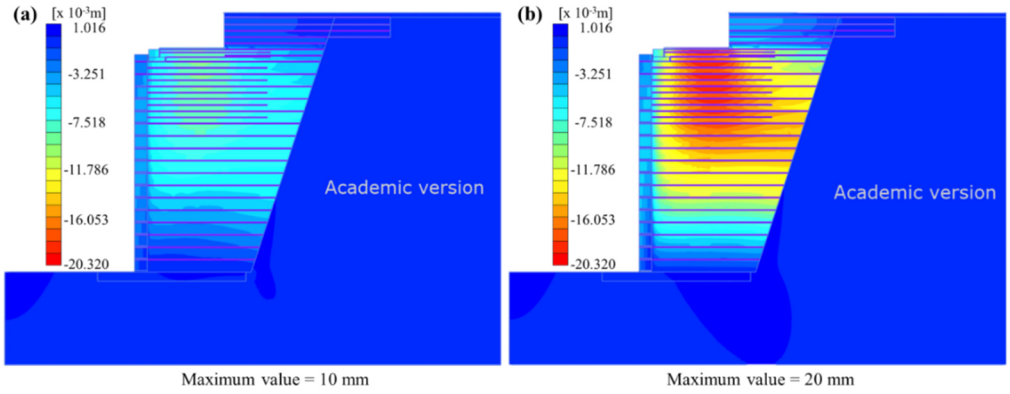


**Figure 12.** Vertical displacement contour for (a) Mohr-Coulomb and (b) Hardening Soil models.

## 5.3. Lateral Displacement

Figure 13 shows the cumulative lateral deformation from the simulations. The lateral deformation according to the US FHWA guidelines is given as twice the vertical displacement assuming a triangular lateral deformation envelop and zero volume change conditions (Adams et al. 2012) and is limited to 1% of the wall height. This estimation is based on vertical deformation which is based on vertical stresses due to the dead load before the bridge is open, hence, results are presented herein for lateral deformations due to dead loads, and then after application of traffic loads.

The maximum lateral deformations from the dead loads were 7.88 mm and 16.00 mm, which were about 0.22% and 0.44% of the abutment height for the MC model and the HS model respectively, both less than the 1% limit recommended by the United States Federal Highway Administration (US FHWA) guidelines (Adams et al. 2012).

The maximum lateral deformations from all construction stages until the structure was opened to traffic were 8.89 mm and 17.78 mm, which were about 0.21% and 0.42% of the GRS-IBS height for the MC

model and the HS model respectively, again, less than the 1% limit recommended by the US FHWA guidelines (Adams et al. 2012).

Figure 14 shows the lateral deformation contours for the two soil models. Both models show very similar deformation patterns with most of the deformations occurring within the middle third of the abutment height. The HS model, again, produced magnitudes about twice that of the MC model, and as stated for the settlement results, the HS model strains about twice as much as the MC model for the observed stress ranges.

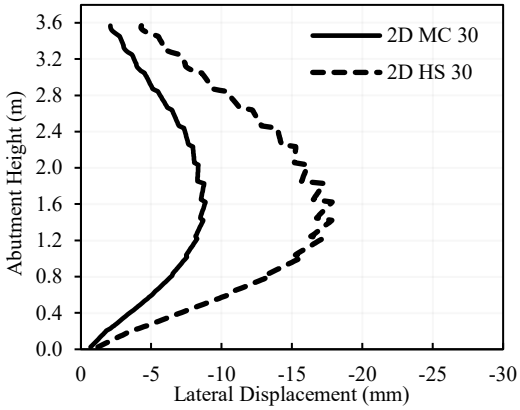


**Figure 13.** Facing lateral displacement versus abutment height

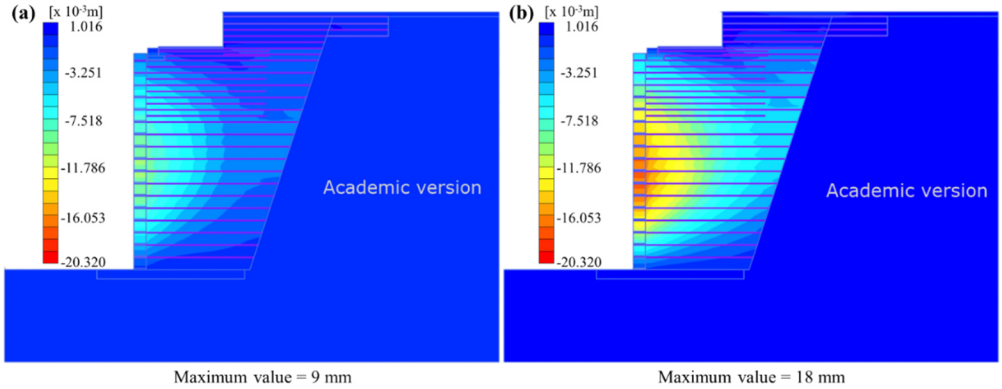


**Figure 14.** Facing lateral displacement contours for (a) Mohr-Coulomb and (b) Hardening Soil models

**Figure 15.** Geosynthetic tensile force vs distance from facing.

### 5.4. Geosynthetic Reinforcement

The tensile forces in the geosynthetic reinforcement are typically very small due to stress redistribution (Adams et al. 2012). The maximum tensile forces in the geosynthetic reinforcement layers occurred in the 8th layer (counting from the concrete pad) for both constitutive models. Figure 15 shows the tensile forces in the 8th reinforcement layer for the two soil models, the maximum value for the MC model was 2.9 kN/m and was 4.3 kN/m for the HS model.

The higher tensile force observed in the HS model compared to the MC model is likely because the HS model depicted higher strains within the reinforced backfill. Observations have shown that the backfill material and the reinforcement strain together due to the confinement provided by the closely spaced reinforcement (Adams et al. 2012, Wu and Adams 2007). The strains were calculated by dividing the tensile force by the reinforcement stiffness (since $N_1 = EA_1\varepsilon_1$ and $N_2 = EA_2\varepsilon_2$, Bentley 2021a). The maximum calculated strain for the MC model was 0.67% and was 0.98% for the HS model.

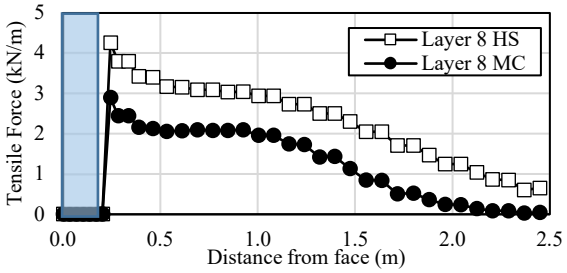


## 6. Conclusion

The objective of this study was to understand the effect of the choice of backfill constitutive models on the numerical simulation of a geosynthetic reinforced soil-integrated bridge system (GRS-IBS). The backfill material was a crushed granite stone with angular shaped fragments, effective grain size of 2.5 mm and maximum aggregate size of 9.5 mm. Laboratory tests were conducted to determine the properties of the backfill material. The backfill was modelled using both the linear-elastic perfectly-plastic (Mohr-Coulomb) and the non-linear Hardening Soil Model. Numerical calibrations were conducted with both models simulating the laboratory configurations. Construction, monitoring, and field results were documented in previous studies. The models were then used in the numerical analyses of the Marshal County GRS-IBS, with lessons learned summarized as follows:

- The numerical analyses result showed good agreement with field measured vertical stresses. The choice of constitutive model did not have a significant effect on the stresses developed within the backfill. This is because the backfill remained elastic during the simulations.
- The maximum settlement due to the dead loads were 0.22% and 0.45% of the abutment height for the Mohr-Coulomb model and the Hardening Soil model respectively, both were less than the 0.5% limit recommended by US FHWA.

- Most of the settlements occurred within the bearing bed reinforcement zone.
- The maximum lateral deformation due to the dead loads were 0.22% and 0.44% of the abutment height for the Mohr-Coulomb model and the Hardening Soil model respectively and were less than the recommended limit of 1%.
- The maximum tensile forces in the geosynthetic reinforcement layers occurred in the 8th layer (counting from the concrete pad) and was 2.9 kN/m for the MC model and 4.3 kN/m for the HS model, resulting in a tensile strain of 0.67% and 0.98% for the MC model and the HS model respectively.

Results from the numerical analyses agreed closely to the field observed vertical stresses. Generally, the stress patterns and magnitudes were consistent between the two models with the maximum magnitude from the HS model being slightly lower (about 8%) than both the MC model and observed value. The HS model consistently produced vertical deformations, lateral deformations, and shear strains that were twice as large as the MC model. This difference is expected as the HS model requires twice as much strain to reach the same stress level in the stress range observed in the backfill.

The results from both soil models are consistent with the observations during and after construction. For the current analyses, the linear elastic model with Mohr-Coulomb failure criterion sufficiently predicts wall performance while eliminating the need for calibrating additional model parameters and is recommended for similar problems with similar ranges of stresses. The vertical stresses from both measurements and the simulations are lower than expected for a one-dimensional stress condition using the height and backfill unit weight. This is believed to be caused by both the interaction of the backfill and the reinforcement and the backfill and the retained rock cutslope. This is currently being explored using three-dimensional models to understand the factors that cause these low stresses.

## Acknowledgements

This work was funded by the Alabama Department of Transportation (ALDOT) through grant number 930-944 and through the Auburn University Highway Research Center. Kaye Davis – Deputy Materials Engineer for ALDOT was instrumental in the success of the project. Robert Pirando-Marshall County Engineer designed and oversaw construction of the bridge simulated in this study and provided assistance with the monitoring. Collection of monitoring data both during and after construction was primarily performed by Jonathan Hogan and Jeffrey Stallings and document in their theses. This assistance and support is gratefully acknowledged. Any opinions, findings, or recommendations expressed herein are those of the authors and should not be interpreted as representing the official policies, either expressed or implied, of the above organizations or individuals.

## References

Adams, M., Nicks, J., Stabile, T., Wu, J., Schelatter, W. and Hartmann, J. (2012). "Geosynthetic Reinforced Soil Integrated Bridge System Interim Implementation Guide." Publication No. FHWA-HRT-11-026, Federal Highway Administration, Washington, DC.

Alabama Department of Transportation (ALDOT) (2017). "Plans of Proposed Project No. BRZ-4814 (251): Marshall County Bridge Replacement and Approaches on Cochran Road at Turkey Creek with GRS-IBS. Montgomery, Alabama.

Bentley (2021a). "Plaxis 3D: Material Models Manual." Plaxis connect edition v21.01. Last updated: March 04, 2021. https://communities.bentley.com/cfs-file/__key/communityserver-wikis-components-files/00-00-00-05-58/PLAXIS3DCE_2D00_V21.01_2D00_03_2D00_Material_2D00_Models.pdf

Bentley (2021b). "Plaxis 3D: Reference Manual." Plaxis connect edition v21.01. Last updated: March 04, 2021. https://communities.bentley.com/cfs-file/__key/communityserver-wikis-components-files/00-00-00-05-58/PLAXIS3DCE_2D00_V21.01_2D00_02_2D00_Reference.pdf

Hatami, K., and Bathurst, R.J. (2005). "Development and Verification of a Numerical Model for the Analysis of Geosynthetic-Reinforced Soil Segmental Walls under Working Stress Conditions." *Canadian Geotechnical Journal*, 42(4), doi:10.1139/T05-040

Hogan, R. J. (2018). "Monitoring and Evaluation of Alabama's First Geosynthetic Reinforced Soil-Integrated Bridge System." Master of Civil Engineering Project, Auburn University, Auburn AL.

Hogan, R. J., Pirando, R., Anderson, J. B. and Montgomery, J. (2019). "Monitoring and Evaluation of Alabama's First Geosynthetic Reinforced Soil-Integrated Bridge System." *Geo-Congress 2019* GSP 306.https://ascelibrary.org/doi/pdf/10.1061/9780784482087.020

Micha Van der Sloot (2018). "Plaxis Soiltest" *Calibration Software.* https://soilmodels.com/soiltest/#:~:text=The%20SoilTest%20option%20is%20a,a%20complete%20finite%20element%20model

NAVFAC, 1982. "Foundations and Earth Structures." *Design Manual* 7.02 86. Department of the Navy Facilities Engineering Command, Alexandria, Virginia 22332-2300. https://web.mst.edu/~rogersda/umrcourses/ge441/DM7_02.pdf

Okafor, C., C., Anderson, J., B., Montgomery, J., Stallings, J., and Hogan., J., R. (2023). "3D modelling of the effects of backfill-retained rock frictional interface on the performance of GRS-IBS." *Manuscript under preparation.*

Stallings, J. (2020). "Implementation of Geosynthetic Reinforced Soil – Integrated Bridge System (GRS-IBS) Technology in Alabama." *M.Sc. thesis, Auburn University*, Auburn AL.

Wood, D. M. (2014). *Geotechnical Modelling*. CRC Press, Florence.

Wu, J., T., H., and Adams, M., T. (2007). "Myth and Fact on Long-Term Creep of GRS Structures," *Geotechnical Special Publication No. 165*, Geosynthetics in Reinforcement and Hydraulic Applications, Proceedings, Geo-Denver 2007, American Society of Civil Engineers, Denver, CO.